

ISTITUTO NAZIONALE DI FISICA NUCLEARE

Sezione di Padova

INFN/BE-85/5  
21 Novembre 1985

G. Nardelli and G. Torielli:  
A STUDY OF THE  $^{89}\text{Y}(n,n'\gamma)^{89}\text{Y}$  REACTION

Servizio Documentazione  
dei Laboratori Nazionali di Frascati

Istituto Nazionale di Fisica Nucleare  
Sezione di Padova

INFN/BE-85/5  
21 Novembre 1985

**A STUDY OF THE  $^{89}\text{Y}(n,n'\gamma)^{89}\text{Y}$  REACTION**

G. Nardelli and G. Tornielli  
Dipartimento di Fisica, Università di Padova and INFN - Sezione di Padova,  
Padova, Italy

**ABSTRACT**

Energy levels of  $^{89}\text{Y}$  were populated by the  $^{89}\text{Y}(n,n'\gamma)$  reaction at neutron energies between 2.2 and 4.8 MeV. A time gated (HP)Ge spectrometer was used to detect the de-excitation  $\gamma$ -rays. Forty-three levels through 4537 keV excitation energy were identified in this way, two of which were previously unreported. Spins and parities were determined within the framework of the statistical theory from the angular distributions and excitation functions of the observed  $\gamma$ -rays. A complete level and decay scheme for  $^{89}\text{Y}$  up to an excitation of 4.32 MeV is presented.

## 1. - INTRODUCTION

As part of a research programme concerning  $(n,n'\gamma)$  studies of some medium-weight nuclei <sup>(1)</sup><sup>(2)</sup> we present in this paper the results of  $^{89}\text{Y}(n,n'\gamma)$  experiments undertaken in order to obtain further information on the spins and parities of energy levels in  $^{89}\text{Y}$  and to extend the knowledge of the gamma decay mode of this nucleus.

Previous work on  $^{89}\text{Y}$ , as reported in the compilation of D.C. Kocher <sup>(3)</sup>, includes a large variety of experimental investigations which have contributed a large body of data for levels below 5 MeV. Information on the level structure is mainly based on the study of  $^{89}\text{Y}(p,p')$  <sup>(4)</sup><sup>(5)</sup>,  $^{89}\text{Y}(d,d')$  <sup>(6)</sup>,  $^{89}\text{Y}(\alpha,\alpha')$  <sup>(7)</sup>,  $^{89}\text{Y}(n,n')$  <sup>(8)</sup> and  $^{89}\text{Y}(n,n'\gamma)$  <sup>(9)</sup><sup>(10)</sup><sup>(11)</sup> reactions. Additional experimental information improving the knowledge of the energy level structure and decay mode of high spin states of the  $^{89}\text{Y}$  nucleus may be found in refs. <sup>(12)</sup><sup>(13)</sup>. Many spin assignments have been made for levels in  $^{89}\text{Y}$ , but information regarding the  $\gamma$ -decay mode is still incomplete above 3 MeV of excitation energy, when not missing completely. Kocker's compilation includes a tentative gamma decay and energy level scheme up to an excitation energy  $E_x \approx 4$  MeV determined from a preliminary  $^{89}\text{Y}(n,n'\gamma)^{89}\text{Y}$  study <sup>(14)</sup>, for which subsequent full publication did not occur.

Substantial discrepancies indeed exist, above 2.5 MeV, between some of the proposed spin and parity assignments and those from the high-resolution  $(p,p')$  experiments of L. Hulstman *et al.* <sup>(5)</sup>. The scheme, too, appears incomplete. It was therefore decided to carry out a  $^{89}\text{Y}(n,n'\gamma)$  experiment measuring  $\gamma$ -ray differential production cross sections and angular distributions in the incident neutron-energy range of 2.2 to 4.8 MeV.

The results of the experiment have been interpreted in the framework of the statistical compound nucleus (CN) reaction theory of Hauser and Feshbach <sup>(15)</sup> and on the basis of Satchler's theory <sup>(16)</sup>. The comparison, in regard to both the shape of the angular distribution and magnitude of the differential cross sections for the  $\gamma$ -rays observed can indeed provide a basis for the choice of level spin and parity assignments.

Measurement of angular distributions of neutrons elastically and inelastically scattered from  $^{89}\text{Y}$  was also undertaken in order to establish an optical potential which would be representative over the wide range of incident energy covered in this experiment and would furnish the transmission coefficients required in Hauser-Feshbach (HF) calculations.

In the present work, the energy level structure and decay modes of  $^{89}\text{Y}$  have been determined up to an excitation energy  $E_x \approx 4.5$  MeV. Some preliminary results of the present experiment have been published elsewhere <sup>(17)</sup>. Most of the results presented there have been confirmed in the subsequent work of ref. <sup>(11)</sup>.

2. - EXPERIMENTAL PROCEDURES AND DATA REDUCTION

The measurements were performed at the Laboratori Nazionali di Legnaro (LNL, Padova) using the 7 MV Van de Graaff accelerator.

A 143 g sample of 99.9% pure elemental yttrium ( $^{89}\text{Y}$ ) in the shape of a solid cylinder 4.5 cm in length and 3.0 cm in diameter was suspended with its symmetry axis perpendicular to the reaction plane at an angle of  $0^\circ$  with respect to the incident charged beam. The distance of the sample from the neutron source ranged from 7.5 to 10 cm for various experimental runs.

Neutrons with energies of from 1.6 to 4.0 MeV were produced by proton bombardment of tritium ( $0.78 \text{ Ci/cm}^2$ ) embedded in metallic Ti. At the lowest neutron energy the energy spread at the sample was  $\pm 45 \text{ keV}$ .

Neutrons with energies of from 3.8 to 4.8 MeV were produced via the  $\text{D}(\text{d},\text{n})^3\text{He}$  reaction using a deuterium-titanium target ( $0.21 \text{ cm}^3/\text{cm}^2$ ) with a maximum energy spread for the neutrons of  $\pm 85 \text{ keV}$ .

During each run the neutron yield was monitored with a neutron time-of-flight spectrometer employing a NE213 liquid scintillator detector 7.5 cm thick and 5 cm in diameter, located 5 m from the neutron source at an angle of  $30^\circ$  with respect to the incident beam. The charge collection was monitored by means of a current integrator of the beam. The de-excitation  $\gamma$ -rays were observed by a (HP)Ge detector of about 18% efficiency and

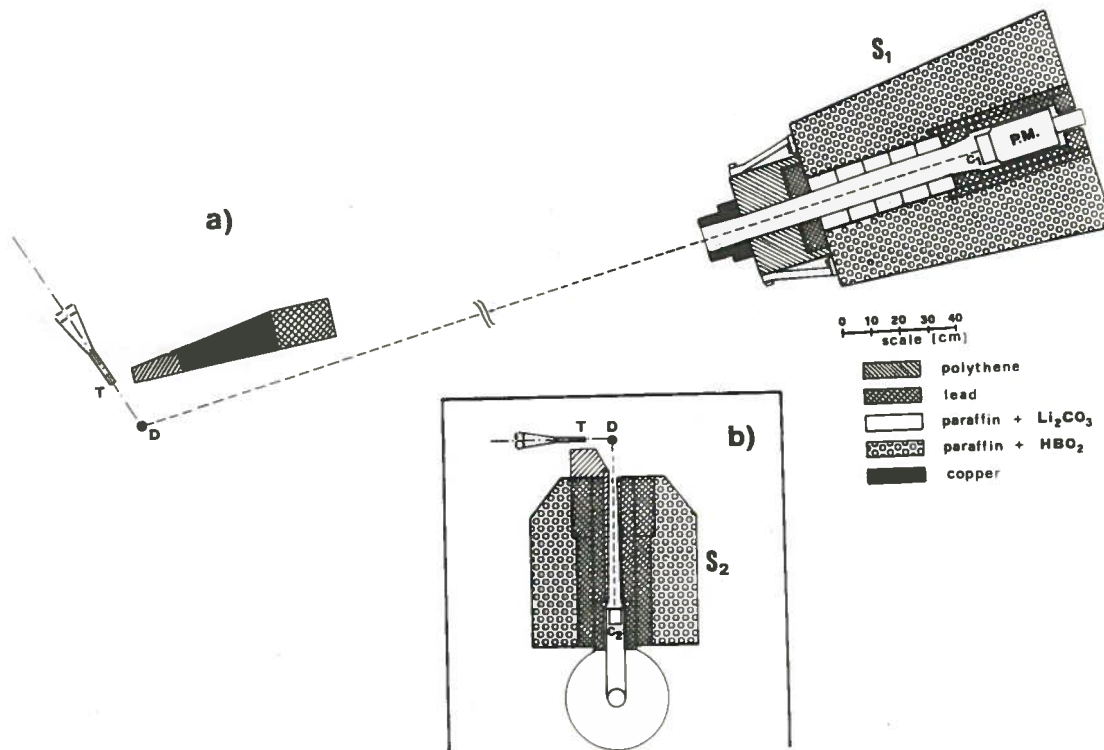


Fig.1- Experimental arrangement.

2.3 keV resolution at 1.33 MeV, placed at an angle of  $90^\circ$  with respect to the beam direction. In order to minimize background radiation in the energy spectra and to protect the Ge-crystal from the direct neutron flux, the detector was collimated and protected by massive shields [Fig. 1,b)].

A 3 ns pulsed beam and a flight path of 0.6 m permitted standard time-of-flight gating techniques (<sup>18</sup>), for n- $\gamma$  discrimination. At each energy the measurement consisted of a spectrum from the Y sample; a spectrum from a carbon sample for identification of background peaks arising from neutron interactions in the Ge detector; and a third spectrum from a sample of natural Fe for relative standardization to  $^{56}\text{Fe}(n,n'\gamma)^{56}\text{Fe}$  cross sections.

The spectra were recorded on a 4096-channel analyser and then processed on a HP1000 computer with an automatic peak fitting code developed in this laboratory (<sup>19</sup>).

In Fig. 2 we show the time-gated energy spectrum, obtained with incident neutrons of maximum energy 4.8 MeV, and recorded with a dispersion of 1.3 keV/channel. Only the lines coming from the  $^{89}\text{Y}(n,n'\gamma)$  reaction are labelled by their energy in keV. The gain and the stability of the electronics were continuously checked using the 2222.5 keV  $\gamma$ -ray from the  $^1\text{H}(n,\gamma)^2\text{H}$  reaction that occurred in the paraffin wax used to shield the Ge detector. The relative efficiency of the 84 cm<sup>3</sup> (HP)Ge detector and the nonlinearity of the analyser were determined using the accurately known relative intensities and energies (<sup>20</sup>) of  $\gamma$ -rays from the radioactive sources  $^{152}\text{Eu}$  and  $^{56}\text{Co}$  or originated by the de-excitation of  $^{28}\text{Si}$  produced in the  $^{27}\text{Al}(p,\gamma)^{28}\text{Si}$  reaction at a proton resonance energy  $E_p=992$  keV (<sup>21</sup>).

Photopeak yields obtained in the analysis of the spectra were corrected for dead time of the electronics and for  $\gamma$ -ray attenuation in the sample using the absorption coefficients given in ref. (<sup>22</sup>). Neutron attenuation and multiple scattering effects have also been taken into account, according to ref. (<sup>23</sup>), using the cross sections for neutrons obtained from ref. (<sup>24</sup>). The excitation functions at  $90^\circ$  of the absolute differential cross sections of the  $^{89}\text{Y}$   $\gamma$ -rays were calculated by normalization of the corrected  $\gamma$ -yields from this nucleus to the photopeak intensities, corrected in the same way, of the 847-keV  $\gamma$ -ray from the  $^{56}\text{Fe}(n,n'\gamma)^{56}\text{Fe}$  reaction, of known production cross sections (<sup>25</sup>)(<sup>26</sup>)(<sup>27</sup>).

A rms combination of the resulting uncertainties with the assigned (<sup>26</sup>),  $\pm 7\%$  uncertainty in the 847-keV production cross section gives the absolute uncertainty in  $\sigma_\gamma(E,90^\circ)$ .

Experimental angular distributions for the  $\gamma$ -rays observed in the present study have been measured at  $E=3.4,3.7,4.2$  MeV at angles between  $30^\circ$  and  $110^\circ$  to the incident

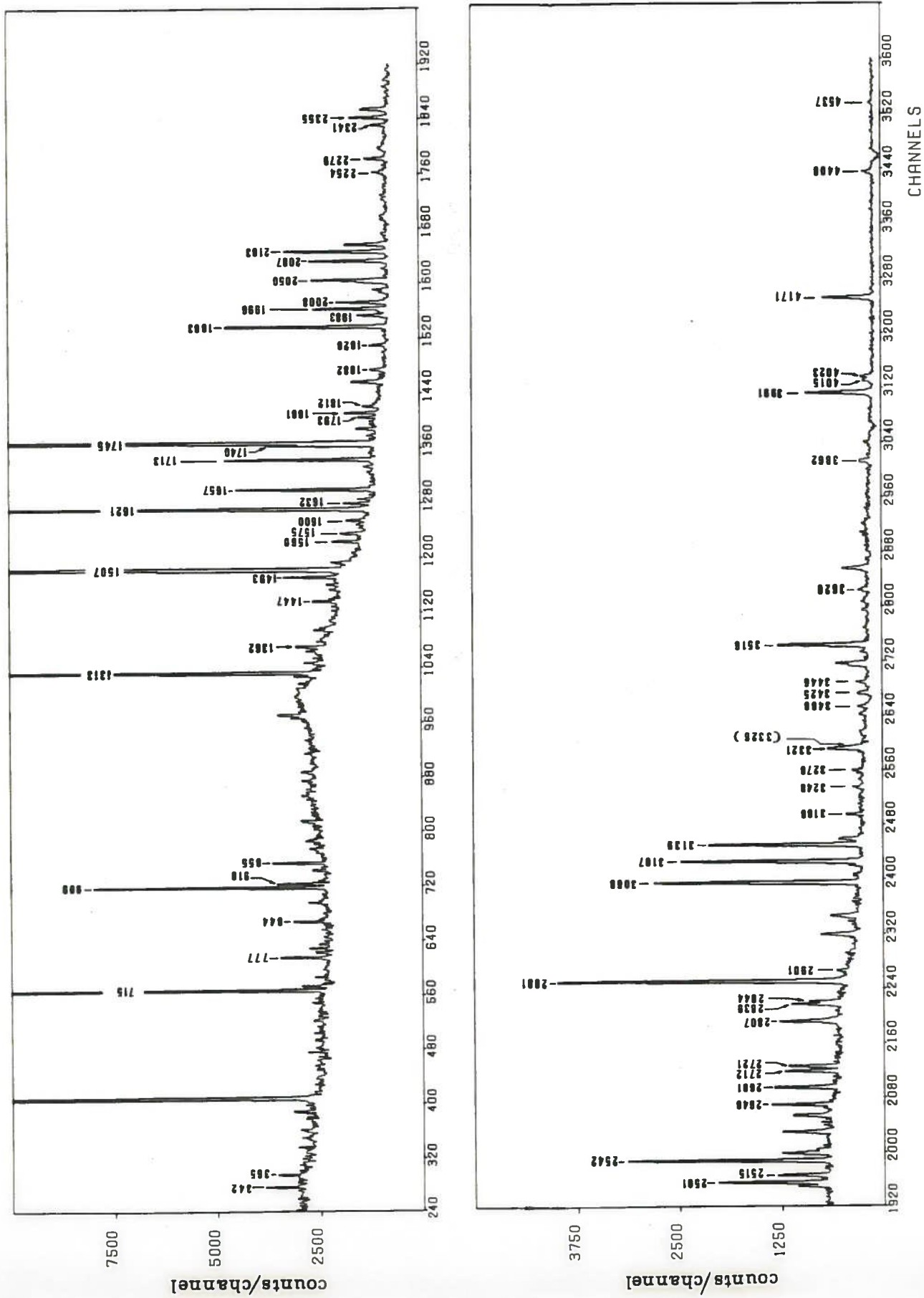


Fig. 2- A  $^{89}\text{Y}(n,n'\gamma)^{89}\text{Y}$  spectrum obtained at  $\theta=90^\circ$  and  $E=4.8$  MeV. A monitor-normalized spectrum has been subtracted. Gamma-ray energies are in keV.

beam direction, and at angles between  $70^\circ$  and  $150^\circ$  at  $E=4.5$  MeV.

The elastic and inelastic neutron cross section measurements were performed by using the time-of-flight facility of the (LNL) laboratory. An arrangement of the experimental apparatus is depicted schematically in Fig. 1,a).

The neutron source was the  $T(p,n)^3\text{He}$  reaction pulsed for duration of  $\approx 2$  ns at a repetition rate of 3 MHz. The target introduced a neutron maximum energy spread of about  $\pm 50$  keV. The scattering yttrium sample was the same as the one used in  $(n,n'\gamma)$  experiments and was placed at 15 cm from the target with neutrons incident on its lateral surface. The scattered-neutron flight paths were 3.9 m. The neutron detector was a NE213 liquid scintillator 5 cm thick and 10 cm in diameter equipped with a pulse shape discrimination circuitry and with the threshold set at approximately 0.8 MeV neutron energy.

A 70-cm-long shadow bar was used to shield the detector from neutrons coming directly from the source and a massive collimator was used in order to reduce as much as possible both the time-correlated and -uncorrelated background in the TOF spectra. The time-of-flight spectra of neutrons scattered by Yttrium were measured at the incident neutron energies of 1.98, 2.50 and 3.02 MeV and at angles of between  $15^\circ$  and  $165^\circ$  to the incident beam direction. Fig. 3 represents a typical time-of-flight spectrum of 3.02 MeV neutrons scattered at  $60^\circ$ . The monitor-normalized background spectrum obtained with the Y-sample removed has been subtracted point by point.

The neutron yield from the target was monitored with the neutron spectrometer used in  $(n,n'\gamma)$  experiments, located at  $0^\circ$  with respect to the incident beam. The relative efficiency of the detector as a function of energy was determined by measuring the neutron yield from the target at  $0^\circ$  using the published cross sections of the  $T(p,n)^3\text{He}$  reaction <sup>(28)</sup>.

The measured angular distributions have been corrected for the effects of flux attenuation in the scattering sample and for neutron multiple scattering <sup>(23)</sup>. All cross

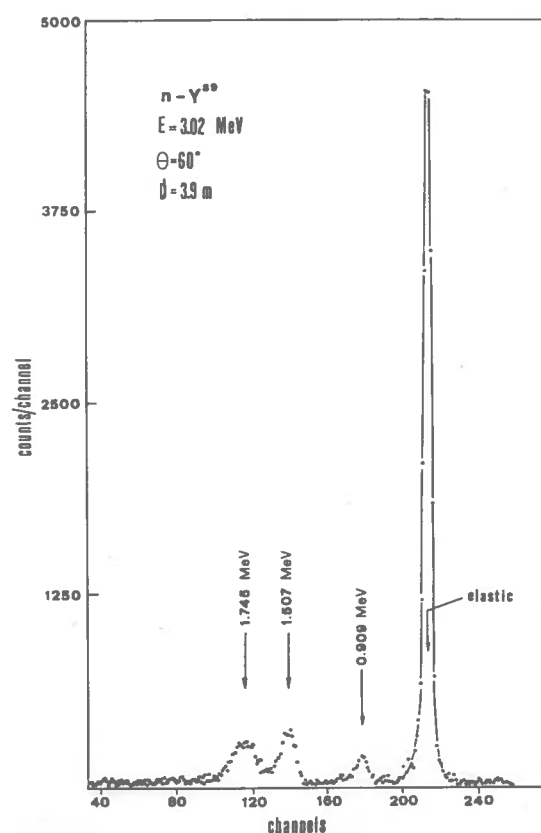


Fig.3- Typical time-of-flight neutron spectrum at  $E=3.02$  MeV (0.95 nsec per channel). The numbers opposite arrows indicate excitation energies;  $d$  is the time-of-flight base.

sections were determined relative to those of neutron scattering from  $^{12}\text{C}$  (<sup>29</sup>), by comparison with the spectra of neutrons observed in similar experiments with the Y-sample replaced by a carbon one.

The typical error for a single point in the elastic case is from 5 to 7% whereas a value between 9 and 16% will be obtained for the total error in the inelastic scattering cross sections. Fig. 4 shows the corrected angular distributions of neutrons elastically scattered (dots) and inelastically scattered to low-lying levels at 909, 1507 and 1745 keV (circles).

### 3. - EXPERIMENTAL RESULTS AND DISCUSSION

As pointed out in the introduction the theoretical previsions of the HF theory depend on the choice of the optical-model (OM) potential parameters to be used in the determination of the transmission coefficients for the CN calculations. In a preliminary analysis of data relative to  $\gamma$ -rays de-exciting the low-lying levels of  $^{89}\text{Y}$ , whose spins and parities are well established, we made an attempt to fit the experimental data using the OM parameters of Becchetti and Greenless (<sup>30</sup>) and those of Wilmore and Hodgson (<sup>31</sup>). The cross sections calculated from these two sets of parameters are presented in Figs. 6,7). It is seen from the figures that neither set of parameter values produces cross sections in agreement with the experimental functions. No substantial improvement can be obtained with an inclusion of a spin-orbit interaction term in the potential of Wilmore and Hodgson. In effect a spin-orbit potential depth of 7.0 MeV, as suggested by Perey and Perey(<sup>32</sup>), contributes to lowering the reaction cross sections calculated without spin-orbit interaction by an amount that, in the range of energies covered in this experiment, is only of about 5%. The shape-elastic cross sections are also comparatively insensitive to variations in this parameter.

The potential parameters needed for the generation of transmission coefficients were thus determined from a fit to the elastic scattering data obtained in this experiment.

#### 3.1. - Neutron elastic and inelastic scattering cross sections

The corrected angular distributions have been compared with distributions calculated with a local nuclear optical model potential of standard form with Saxon-derivative surface absorption and without a spin-orbit interaction term. Three of the potential parameters, i.e. the depth  $U$  of the real potential, the depth  $W_D$  and the diffuseness  $a_D$  of the imaginary potential have been adjusted to obtain the best agreement with the measured elastic cross sections. The best fits to the experimental data have been acquired by



using the "ABACUS-2" [ref. (33)] automatic multi-parameter search code. The compound nucleus cross sections were estimated using the Sheldon's (34) "MANDYF" code taking into account the correction for level-width fluctuations [ref. (35)]. A rapid convergence of the fitting procedure was achieved starting from the OM parameters adopted by Towle (8) in his study of the inelastic scattering of neutrons from  $^{89}\text{Y}$  and assuming that only the real-potential strength  $U$  was energy dependent. Table 1 gives the values of the various parameters resulting from the present analysis. Strength  $W_D$ , adopted for the absorptive potential and apparently too small for a nucleus in the region near  $A=90$ , may possibly be associated with the shell closure effects proposed by Lane *et al.* (36). This choice is also supported by the results of Johnson *et al.* (37) predicting a minimum for this strength at the fifty-neutron shell closure.

TABLE 1.- Optical model parameters (depths are in MeV and ranges in fm).  $U$  has the Saxon-Woods form. The radii of the real and imaginary potentials are  $r_r A^{1/3}$  and  $r_D A^{1/3}$ , respectively.  $E$  denotes neutron energy (in MeV).  
a) ref. (8)

	$U$	$W_D$	$r_r$	$r_D$	$a_r$	$a_D$
$n + ^{89}\text{Y}$	$50.0 - 0.5E$	5.9	$1.25^a$	$1.25^a$	$0.65^a$	0.44

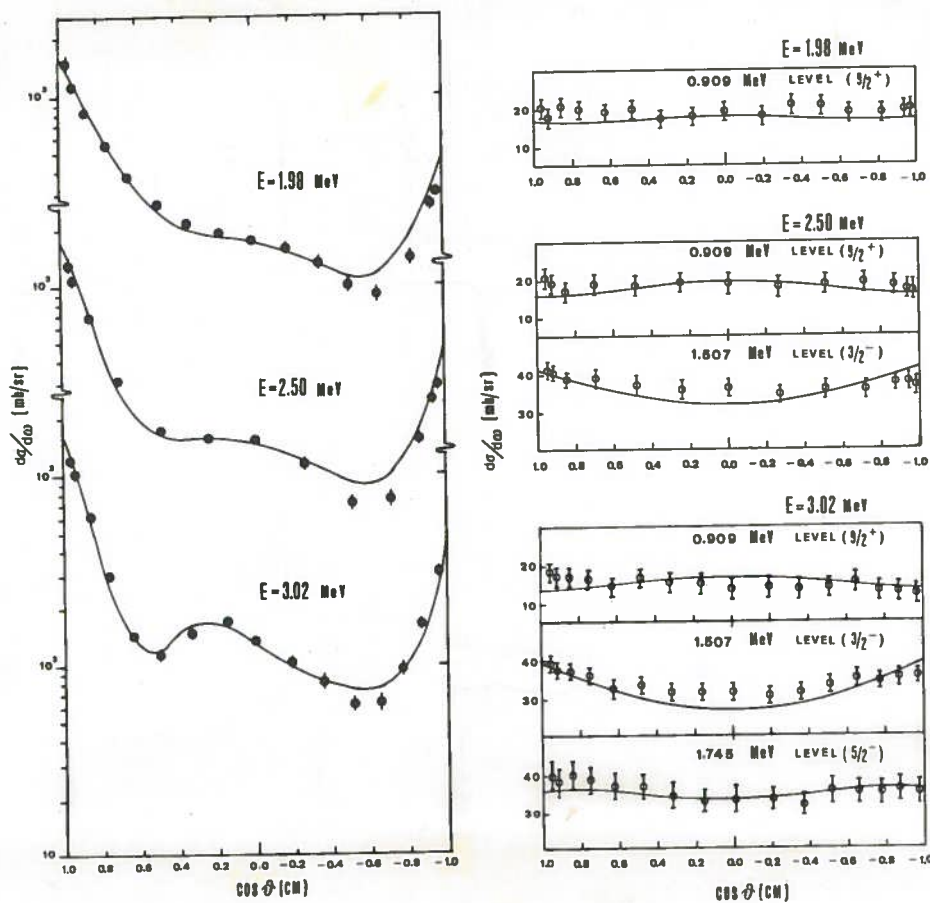


Fig.4-On the left-hand side, the differential cross sections for the elastic scattering of neutrons by  $^{89}\text{Y}$ , for the indicated values of the incident neutron energy. The curves are Optical-Model calculations. On the right-hand side, the differential cross sections from the inelastic scattering to the indicated levels of  $^{89}\text{Y}$ . The vertical bars represent the total uncertainty for each point. The solid curves are theoretical calculations obtained with the Hauser-Feshbach formalism for the indicated spin-values.

On the left-hand side of Fig. 4 the sum of compound and shape-elastic cross sections for the potential obtained in this analysis is compared with the measured values. On the right-hand side of the same figure the measured differential cross sections for the inelastic scattering of neutrons to the first three excited levels of  $^{89}\text{Y}$  are compared with the prediction of the modified Hauser-Feshbach theory. Table 2 summarizes the results of Legendre polynomial fits of experimental data together with the predictions of OM and HF calculations.

TABLE 2.- Integrated cross sections (in mb) for elastic and inelastic scattering of neutrons from  $^{89}\text{Y}$ .  $E_x$  denotes the excitation energy of the level,  $J^\pi$  its spin and parity and  $E_n$  the incident neutron energy. All energies are in MeV. In parenthesis the predictions from optical model and Hauser-Feshbach calculations

$E_x$	$J^\pi$	$\sigma_n$		
		$E_n=1.98$	$E_n=2.50$	$E_n=3.02$
0	$1/2^-$	3659±170 (3770)	3019±140 (3138)	2667±150 (2691)
0.909	$9/2^+$	245±16 (215)	239±15 (229)	190±15 (193)
1.507	$3/2^-$		462±38 (443)	423±35 (401)
1.745	$5/2^-$			454±40 (442)

### 3.2 - Analysis of $\gamma$ -ray excitation functions and angular distributions

The  $\gamma$ -ray yield measurements were performed at  $90^\circ$  with respect to the beam direction for twenty-two neutron energies from 1.7 to 4.7 MeV in steps of circa 100 keV and extrapolated back to threshold to identify the decay level. Sixty-nine  $^{89}\text{Y}(n,n'\gamma)$  gamma rays observed in the present experiment are listed and classified with respect to level of origin in Table 3. Each value reported in the third column of Table 3 is the weighted average from all the spectra measured. The branching ratios, as measured at  $90^\circ$ , are presented in the fourth column as a percentage of total decays and have not been corrected for internal conversion effect, which should be small.

Ambiguities in the  $\gamma$ -ray multiple assignment, made possible by the finite energy resolution of the spectrometer, will be discussed in the next subsection.

The excitation functions of  $\gamma$ -rays from level in  $^{89}\text{Y}$  up to an excitation energy of 4.310 MeV are shown in figs. 6 through 14 (left panels). Error bars represent the absolute errors. For each  $\gamma$ -ray the data, given in absolute values, have been obtained by subtracting the contribution for all cascades feeding the level of origin from the corresponding differential production cross sections. No data for the 0.909 MeV level were obtained with this method due to its metastable nature ( $T_{1/2}=16.6$  sec).

TABLE 3.- Energy levels,  $\gamma$ -ray energies and branching ratios determined in the  $^{89}\text{Y}(n,n'\gamma)^{89}\text{Y}$  measurements.

Initial state (keV)	Final state (keV)	$E_\gamma$ (keV)	Branching ratios (%)	Initial state (keV)	Final state (keV)	$E_\gamma$ (keV)	Branching ratios (%)
909.0±0.3	g.s.	909.0±0.3	100	3747.7±0.9	909	2838.7±0.8	100
1507.2±0.3	g.s.	1507.2±0.3	100	3752.8±0.7	909	2844.2±0.8	23.7±1.7
1744.7±0.4	g.s.	1744.7±0.4	100		1745	2008.3±0.6	68.1±1.8
2222.3±0.4	909	1313.2±0.3	68.5±0.6		3410	341.9±0.5	8.2±0.8
	1507	715.2±0.3	31.5±0.6	3848.1±0.6	1507	2340.8±0.6	15.1±1.2
2529.8±0.4	909	1620.8±0.3	100		1745	2103.5±0.5	84.9±1.2
2566.3±0.5	909	1657.3±0.4	100	3862.1±0.6	g.s.	3861.8±0.9	23.7±1.8
2622.0±0.5	909	1713.0±0.4	100		1507	2355.1±0.5	76.3±1.8
2871.8±0.5	909	1962.8±0.4	100	3976.8±0.7	2530	1447.0±0.5	100
2881.2±0.6	g.s.	2881.2±0.6	100	3991.5±0.8	g.s.	3991.5±0.8	100
2892.5±0.7	909	1983.5±0.6	100	4015.1±1.0	g.s.	4015.4±1.5	57.3±3.6
3067.5±0.5	g.s.	3067.6±0.6	90.4±0.7		2222	1792.8±0.7	42.7±3.6
	1507	1559.8±0.5	9.6±0.7	4022.8±0.7	g.s.	4022.9±1.5	11.5±1.1
3107.2±0.7	g.s.	3107.5±0.6	82.5±1.1		1507	2515.3±0.6	28.8±1.2
	1507	1599.8±0.4	8.4±0.8		1745	2278.6±0.7	22.3±1.2
	1745	1361.8±0.9	9.1±0.7		2222	1800.8±0.4	20.9±1.0
3138.9±0.6	g.s.	3139.2±0.6	77.9±0.9		3067	955.0±0.3	16.5±0.8
	1507	1631.6±0.4	12.7±0.6	4104.9±0.9	909	3196.3±1.2	22.5±2.2
	2222	916.1±0.5	9.4±0.8		2222	1882.5±0.8	32.6±2.5
3247.4±0.6	g.s.	3247.5±0.9	6.9±1.8		2530	1574.9±0.7	41.8±2.6
	1507	1740.2±0.5	93.1±1.8	4170.8±1.1	g.s.	4170.8±1.1	100
3343.3±0.7	2566	777.0±0.4	100	4187.9±0.8	909	3278.7±0.9	16.1±1.8
3410.4±0.6	909	2501.4±0.5	100		1507	2680.9±0.7	83.9±1.8
3451.3±0.7	909	2542.3±0.6	100	4230.4±1.3	909	3321.4±1.2	100
3503.4±0.6	1507	1996.2±0.5	94.1±0.9	4309.1±0.8	909	3400.5±0.9	11.6±1.2
	3139	364.7±0.5	5.9±0.9		2222	2086.7±0.7	88.4±1.2
3516.2±0.8	g.s.	3516.2±0.8	100	4334.1±1.3	909	3425.1±1.2	100
3557.3±0.7	909	2648.3±0.6	37.8±1.5	4354.7±1.1	909	3445.7±1.0	100
	1507	2050.1±0.8	49.8±1.6	4408.2±1.1	g.s.	4408.2±1.3	60.5±4.7
	1745	1812.5±0.9	12.4±1.8		1507	2901.0±1.0	39.5±4.7
3621.1±0.7	909	2712.1±0.6	100	4457.6±0.8	2530	1927.8±0.6	100
3630.4±0.7	909	2721.4±0.6	100	4476.1±1.3	2222	2253.8±1.2	100
3715.1±0.5	909	2806.7±0.8	47.3±2.3	4529.3±1.6	909	3620.3±1.6	100
	2222	1492.7±0.4	38.0±1.9	4537.4±2.0	g.s.	4537.4±2.0	100
	2872	843.6±0.5	14.7±1.1				

Angular distributions for the prominent  $\gamma$ -rays observed in this reaction have also been measured at some incident neutron energies above 3.0 MeV. Least-squares fits to the yields and their statistical uncertainties were made with even-order Legendre polynomial expansions of the form  $\sigma(\theta) = a_0 [1 + \sum_{\nu} a_{\nu} P_{\nu}(\cos\theta)]$ . The angle-integrated production cross sections  $\sigma_{\gamma}(E_n, E_{\gamma}) = 4\pi a_0$  obtained from the fits are listed in Table 4. On the right-hand side of Figs. 6 through 14 some angular distributions are reported as angular asymmetries  $W(\theta) = \sigma(\theta) / \sigma(90^\circ)$ . The error bars include yield and monitor uncertainties but do not include the uncertainty due to absolute normalization.

CN theoretical calculations of excitation functions and angular distributions for each  $\gamma$ -ray have been carried out by means of a version of the "MANDYF" code, developed in this laboratory, containing provision for linear interpolation of the neutron-transmission coefficients to be used in the Hauser-Feshbach calculations, for a series of values of the input parameters. Entry-sets of transmission coefficients were computed externally with the "ABACUS-2" code on the basis of our OM analysis of elastic data. The calculations, performed on a CDC 7600 series machine, were made taking into account the Moldauer level-width fluctuation correction, assuming a partial-wave cutoff at  $l_{\max} = 6$  and starting with the level spin-sequence reported in the high-resolution  $^{89}\text{Y}(p,p')$  experi-

TABLE 4. - Angle-integrated  $\gamma$ -ray production cross sections.  $\sigma_{\gamma}(E_n, E_{\gamma})=4\pi a_0$  (in mb).

Level (keV)	$E_{\gamma}$ (keV)	$E_n=3.4$ MeV	$E_n=3.7$ MeV	$E_n=4.2$ MeV	$E_n=4.5$ MeV
1507.2	1507.2	447±40	433±36	382±35	357±31
1744.7	1744.7	379±29	330±25	278±23	239±18
2222.3	1313.2	90±9	85±8	88±8	87±7
	715.2	38±3	35±3	36±3	35±3
2529.8	1620.8	86±8	86±7	85±7	88±7
2566.3	1657.3	13±2	19±2	24±2	26±3
2622.0	1713.0	34±4	41±4	39±4	35±3
2871.8	1692.8	48±7	60±8	53±7	51±5
2881.2	2881.2	136±14	129±14	105±11	79±8
2892.5	1983.5			5±1	6±1
3067.5	3067.6	72±8	87±8	81±7	65±5
	1559.8			11±2	8±2
3107.2	3107.5	75±8	91±10	79±8	66±5
	1599.8		8±2	6±1	5±1
	1361.8			7±1	6±1
3138.9	3139.2	58±7	86±8	81±7	61±5
	1631.6			10±2	9±1
	916.1		9±2	8±1	7±1
3247.4	1740.2			40±8	38±7
3343.3	777.0			5±2	4±1
3410.4	2501.4		41±6	40±6	33±5
3451.3	2542.3			58±7	46±5
3503.4	1996.2			38±4	31±3
3516.2	3516.2			43±5	42±5
3557.3	2648.3			14±2	13±2
	2050.1			20±3	21±3
	1812.5				7±2
3621.1	2712.1			12±2	12±2
3630.4	2721.4			11±2	12±2
3715.1	2806.7			10±2	13±2
	1492.7				10±2
3747.7	2838.7			12±2	14±2
3752.8	2844.2				7±1
	2008.3			18±3	20±3
	341.9				3±1
3848.1	2340.8				6±1
	2103.5			21±4	27±4
3862.1	3861.8				7±2
	2355.1			14±3	19±4
3991.5	3991.5			16±3	51±7
4015.1	1792.8				5±1
4022.8	2515.3			7±2	15±2
	2278.6				12±3
	1800.8				10±2
	955.0				8±2
4104.9	3196.3				3±1
	1882.5				4±1
4170.8	4170.8				38±6
4187.9	2680.9				13±2
4309.1	2086.7				14±2

ment (5). No correction was applied for contribution of the extra exit channels  $^{89}\text{Y}(n,p)$   $^{89}\text{Sr}(Q=-0.69\text{ MeV})$ ,  $^{89}\text{Y}(n,\alpha)$   $^{89}\text{Rb}(Q=0.31\text{ MeV})$  and  $^{89}\text{Y}(n,\gamma)$   $^{90}\text{Y}(Q=6.85\text{ MeV})$  because of their relatively small cross sections (38) over the energy-range covered by this experiment. Effects of cascading from higher levels on the shapes of the angular distributions were taken into account for levels above 2.5 MeV of excitation energy. Below this energy such a correction seems meaningless owing to the large number of observed cascade transitions feeding the low lying excited levels and because of the limited accuracy of our angular distribution measurements. For the gamma rays which were calculated as other than pure transitions an attempt was made to extract the adjustable parameter  $\delta$  which defines the  $\gamma$ -multipole mixture ratio, from the angular distribution fit. The results of this search are furnished by the aforementioned "MANDYF" code using the methods and conventions of Sheldon and Van Patter (39). In the case of a double-valued solution for  $\delta$  the lower absolute value of this parameter has been systematically adopted. In the left panels of Figs. 6 through 14 the curves represent the excitation functions calculated from the HF theory for the spins indicated. It can be seen from the figures that, in general, the predicted cross sections for excitation of states of the same spin but opposite parity differ quite markedly. A possible explanation of the enhancement of the Hauser-Feshbach penetrability term  $\tau$  (15) for negative-parity states with respect to positive-parity ones may lie, as suggested by Shafroth *et al.* (9), in the fact that  $^{89}\text{Y}$  is near the peak of the p-wave strength function resonance.

It is well known that for an excited state populated near threshold via a  $(n,n'\gamma)$  reaction and for which the spin  $J > |J_0 + 1|$ , where  $J_0$  is the spin of the ground state, the magnetic substate population is low. Consequently the anisotropy of the subsequent gamma-ray decay is large. For  $^{89}\text{Y}$  this condition is fulfilled for  $J > 3/2$ . Some examples of predicted anisotropies are reported in the right panels of Figs. 6 through 14.

From the above considerations one may expect that for  $^{89}\text{Y}$  a joint studium of excitation functions and angular distributions can provide reliable tests for spin and parity assignments. The spins and parities which were assumed for each level in the final theoretical calculations were selected on the basis of several trials, the results of which will be presented in the level-by-level discussion to follow.

### 3.3 - Discussion

An energy level digram for  $^{89}\text{Y}$  that agrees with the results of the present study is presented in Fig. 5 and a complete comparison between the previous results and the present work is summarized in Table 5.

TABLE 5. - Comparison between  $J^\pi$  values reported in the literature and obtained in the present work.

- a) The values adopted from the literature and confirmed.  
 b) The assignments among the previous ones which fit best our data.  
 c) The newly proposed assignments.  
 d) Ref. (5). e) Ref. (9). f) Ref. (10). g) Ref. (12). h) Ref. (3).

Energy (keV)		$J^\pi$						
Present work	d)	d)	e)	f)	g)	h)	present work	
909			9/2 <sup>+</sup>	9/2 <sup>+</sup>	9/2 <sup>+</sup>	9/2 <sup>+</sup>	9/2 <sup>+</sup> a)	
1507			3/2 <sup>-</sup>	(3/2 <sup>-</sup> )	3/2 <sup>-</sup>	3/2 <sup>-</sup>	3/2 <sup>-</sup> a)	
1745			5/2 <sup>-</sup>	5/2 <sup>-</sup>		5/2 <sup>-</sup>	5/2 <sup>-</sup> a)	
2222	2221	5/2 <sup>+</sup>	(5/2 <sup>+</sup> )	(7/2 <sup>+</sup> , 5/2 <sup>+</sup> )		5/2 <sup>+</sup>	5/2 <sup>+</sup> b)	
2530	2530	7/2 <sup>+</sup>	(7/2 <sup>+</sup> , 9/2)	(9/2 <sup>+</sup> , 7/2 <sup>+</sup> )	7/2 <sup>+</sup>	7/2 <sup>+</sup>	7/2 <sup>+</sup> b)	
2566	2565	11/2 <sup>+</sup>			11/2 <sup>+</sup>	(11/2 <sup>+</sup> )	11/2 <sup>+</sup> b)	
2622	2621	9/2 <sup>+</sup>	(9/2 <sup>+</sup> )			9/2 <sup>+</sup>	9/2 <sup>+</sup> b)	
2872	2872	(5/2, 7/2) <sup>+</sup>	(3/2 <sup>-</sup> )	(3/2 <sup>-</sup> )		(5/2, 7/2) <sup>+</sup>	7/2 <sup>+</sup> b)	
2881	2882	(3/2, 5/2) <sup>-</sup>				3/2 <sup>-</sup>	3/2 <sup>-</sup> b)	
2893	2893	(13/2 <sup>+</sup> )			(13/2 <sup>+</sup> )		13/2 <sup>+</sup> b)	
3067	3065	3/2 <sup>-</sup>	(5/2 <sup>-</sup> )	(3/2 <sup>-</sup> )		3/2 <sup>-</sup>	3/2 <sup>-</sup> b)	
3107	3105	(3/2, 5/2) <sup>-</sup>			(3/2, 5/2) <sup>-</sup>	(3/2, 5/2) <sup>-</sup>	5/2 <sup>-</sup> b)	
3139	3137	(3/2, 5/2) <sup>-</sup>				(3/2, 5/2) <sup>-</sup>	5/2 <sup>-</sup> b)	
3247	3247						(5/2) <sup>+</sup> c)	
3343					(13/2)		13/2 <sup>+</sup> b)	
3410	3413						5/2 <sup>+</sup> c)	
3451							(7/2 <sup>+</sup> ) c)	
3503	3501			(5/2 <sup>-</sup> )			7/2 <sup>+</sup> c)	
3516	3513	(3/2, 5/2) <sup>-</sup>				3/2 <sup>-</sup>	3/2 <sup>+</sup> b)	
3557	3555					(1/2) <sup>-</sup>	(7/2 <sup>+</sup> ) c)	
3621							11/2 <sup>+</sup> c)	
3630	3629	(9/2, 11/2) <sup>+</sup>				(9/2, 11/2) <sup>+</sup>	11/2 <sup>+</sup> b)	
3715	3717	5/2 <sup>+</sup>				5/2 <sup>+</sup>	5/2 <sup>+</sup> b)	
3748	3750	(9/2, 11/2) <sup>+</sup>				(9/2, 11/2) <sup>+</sup>	9/2 <sup>+</sup> b)	
3753							5/2 <sup>+</sup> c)	
3848	3852						5/2 <sup>+</sup> c)	
3862	3863	(3/2, 5/2) <sup>-</sup>				(3/2, 5/2) <sup>-</sup>	7/2 <sup>+</sup> c)	
3977	3975	(9/2, 11/2) <sup>+</sup>				(9/2, 11/2) <sup>+</sup>	(11/2 <sup>+</sup> ) b)	
3991	3990	(3/2, 5/2) <sup>-</sup>				(3/2, 5/2) <sup>-</sup>	3/2 <sup>-</sup> b)	
4015	4011						(1/2, 3/2) c)	
4023	4020	(3/2, 5/2) <sup>-</sup>				(3/2, 5/2) <sup>-</sup>	3/2 <sup>-</sup> b)	
4105	4104						(7/2 <sup>+</sup> ) c)	
4170	4171	(3/2, 5/2) <sup>-</sup>				(3/2, 5/2) <sup>-</sup>	5/2 <sup>-</sup> b)	
4188	4188	5/2 <sup>+</sup>				(3/2, 5/2) <sup>+</sup>	5/2 <sup>+</sup> b)	
4230	4230						(7/2 <sup>+</sup> ) c)	
4309	4304	(7/2, 9/2) <sup>-</sup>				(7/2, 9/2) <sup>-</sup>	(9/2 <sup>-</sup> ) b)	
4334	4330							
4355	4352							
4408	4404							
4458	4456	(7/2, 9/2) <sup>-</sup>				(7/2, 9/2) <sup>-</sup>		
4476	4473	(5/2 <sup>+</sup> )						
4529	4526	(5/2, 7/2) <sup>+</sup>				(5/2, 7/2) <sup>+</sup>		
4537	4536	(3/2, 5/2) <sup>-</sup>				(3/2, 5/2) <sup>-</sup>		

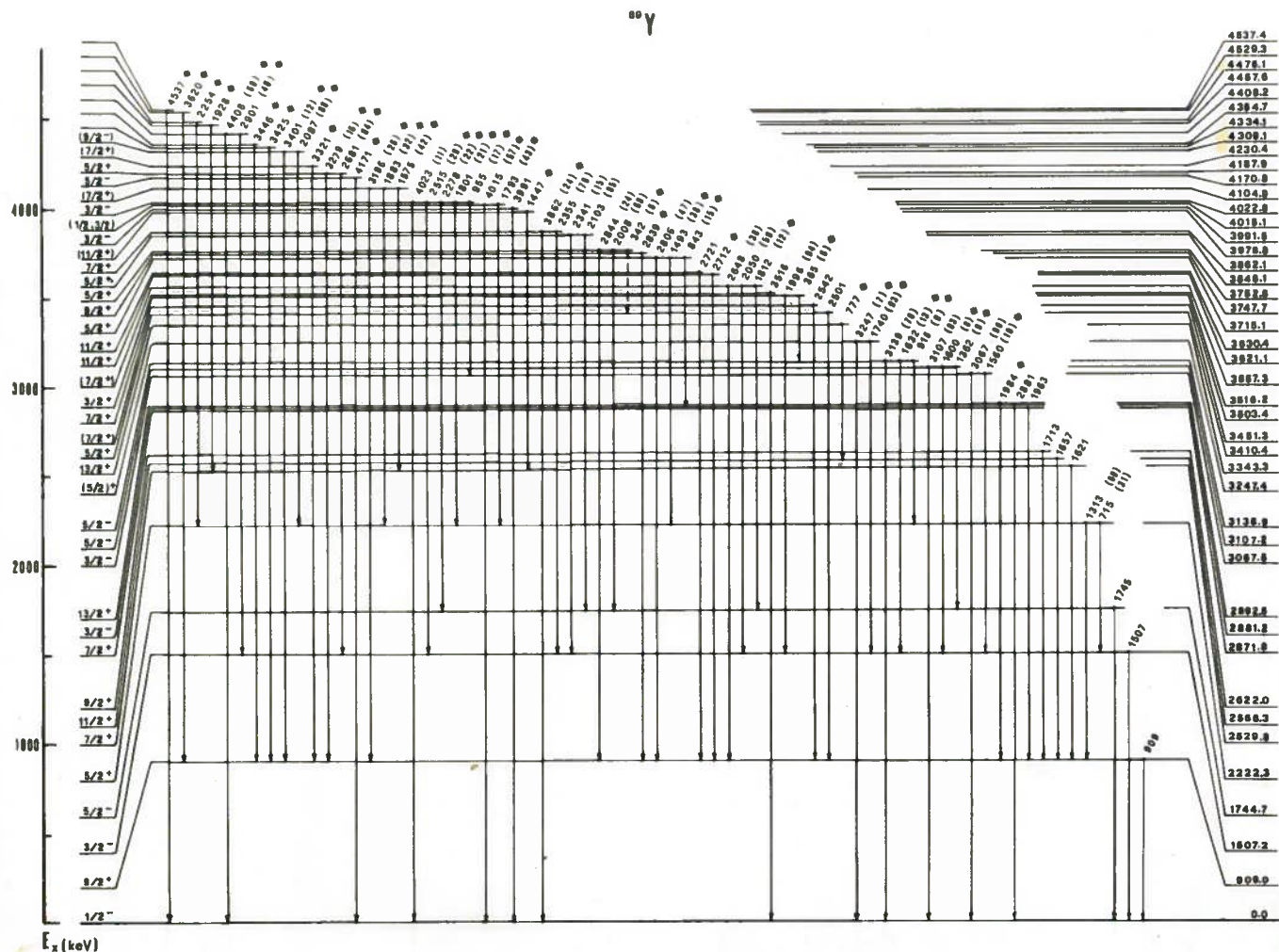


Fig.5-The  $^{89}\text{Y}$  level and decay scheme, showing  $\gamma$ -ray transitions and branching ratios (in parenthesis) observed in the present investigation. Transitions labelled with an asterisk were observed for the first time in the present measurements. Suggested  $J^\pi$  are also indicated.

The experimental results of present direct-neutron measurements for the 909, 1507 and 1745-keV levels are in general agreement with the values obtained by Towle <sup>(8)</sup> and, more recently, by Budtz-Jørgensen *et al.* <sup>(11)</sup>. For these levels the data obtained from combined neutron and gamma-ray measurements are consistent with earlier  $J^\pi$  assignments of  $9/2^+$ ,  $3/2^-$  and  $5/2^-$ , respectively (see Figs. 4,6). The shape of the 1507-keV  $\gamma$ -ray angular distributions is consistent with a mixture of M1 and E2 transitions. Assuming a 67% confidence limit for the uncertainties on  $a_2^*$  and averaging over the various results obtained at the four neutron-bombarding energies we obtain for the multipole mixing ratio the magnitude  $\delta = -0.30_{-0.09}^{+0.12}$ . Our results do not agree with the value  $-2 \leq \delta \leq -2.8$  reported by Buchaman *et al.* <sup>(10)</sup>.

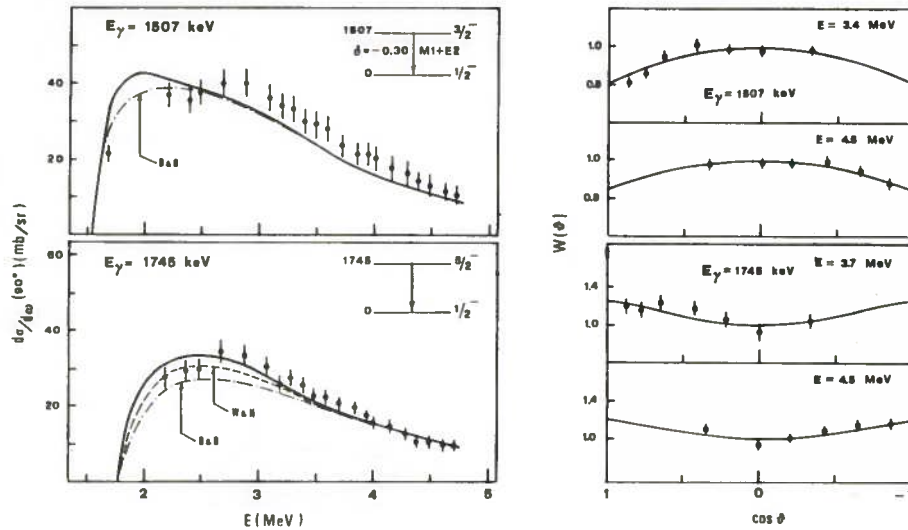


Fig.6-Experimental and calculated excitation functions (left panels) and angular distributions (right panels) of  $\gamma$ -decays from the 1507 and 1745-keV levels. The theoretical cross sections shown as solid lines were obtained using the transmission coefficients calculated on the basis of our Optical-Model analysis of elastic data. The dashed lines represent predictions using the potential parameters of Wilmore-Hodgson (marked W&H), while the dot-dashed lines represent predictions using the potential parameters of Becchetti-Greenless (marked B&G). The adopted spin, parity and  $\delta$ -values are shown in the decay schemes.

The level at  $E_x=2222$  keV. In refs. (5)(8)(9) the suggested spin and parity value for this level is  $5/2^+$  and in ref. (10)  $(7/2, 5/2)^+$ . In the present work, two gamma-rays are found which can be assigned to this level. The measured branching ratio of 31% for the 715 keV decay is in good agreement with the values given in refs. (3)(9)(11). The shape of the experimental angular distributions of the two gamma-rays exclude the  $7/2^+$  assignment, whereas the calculated excitation functions give best agreement with experiment for the  $5/2^+$  choice (Fig. 7).

The level at  $E_x=2530$  keV. For this state the  $(n, n')$  cross sections inferred from our  $(n, n' \gamma)$  measurements (Table 4) are in excellent agreement with those of refs. (8)(11). Several studies [refs. (5)(7)(9)(10)] have narrowed choices for this level to  $J^\pi=7/2^+$ ,  $9/2^+$ . Both the angular distributions presented here for the 1621-keV  $\gamma$ -decay and the excitation function are consistent only with an assignment  $J^\pi=7/2^+$ . The shape of the experimental angular distributions seems to warrant a mixing of M1 and E2 multipolarity (Fig. 7). It should be noted that above 3.5 MeV incident energy the excitation function exhibits a behaviour which seems to outline an incorrect subtraction for cascading from higher levels or a contribution to the 1621 keV line of another unresolved transition. In our decay scheme the latter possibility is restricted to the decay from the 4187.9-keV level to the 2566.3-keV level and is strongly hindered by  $\gamma$ -ray selection rules.



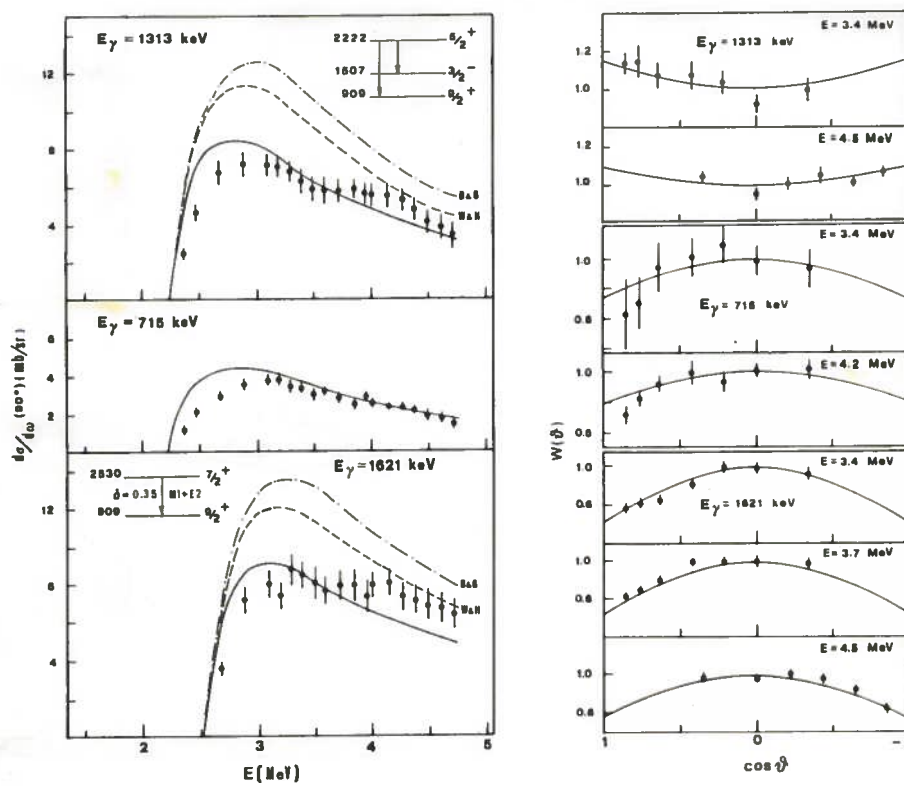


Fig.7-Experimental and calculated excitation functions (left panels) and angular distributions (right panels) of  $\gamma$ -decays from the 2222 and 2530-keV levels. The notations for the curves are the same as in fig.6.

The level at  $E_x=2566$  keV. This level decays only to the 909-keV state. The excitation function and the angular distributions of the 1657-keV  $\gamma$ -ray confirm the  $J^\pi=11/2^+$  assignment of ref.(5).

The level at  $E_x=2622$  keV. The existence of a level at this energy and the accompanying 1705-keV  $\gamma$ -ray was first observed in ref. (9). In ref. (5)  $J^\pi=9/2^+$  has been confirmed. No evidence was found in the present work for a branching (11) of this level to the 1507-keV level (spin  $3/2^-$ ), whereas a single transition to the 909-keV level (spin  $9/2^+$ ) has been observed. Such branching requires a competition of the M1 radiation (the 1713-keV  $\gamma$ -ray) with E3 radiation (the 1115-keV  $\gamma$ -ray) which seems unlikely.

The excitation function of the observed 1713-keV  $\gamma$ -ray is well fitted by the calculations with  $J^\pi=9/2^+$  whereas the large uncertainties in the angular distribution data do not allow for a conclusive analysis (Fig.8).

The level at  $E_x=2872$  keV. Hulstman *et al.* (5) have confirmed the existence of a triplet at 2.88 MeV whose lower level corresponds to the level observed in this work. Their proposal of  $J^\pi=(5/2,7/2)^+$  ( $L=3$ ) for this level conflicts with the  $J^\pi=9/2^+$  of ref. (3). Both the excitation function and the angular distributions presented here for 1963-keV  $\gamma$ -decay are in agreement with an assignment  $J^\pi=7/2^+$  (Fig. 8). The large negative anisotropy of the observed angular distributions seems to warrant M1-E2 mixing.

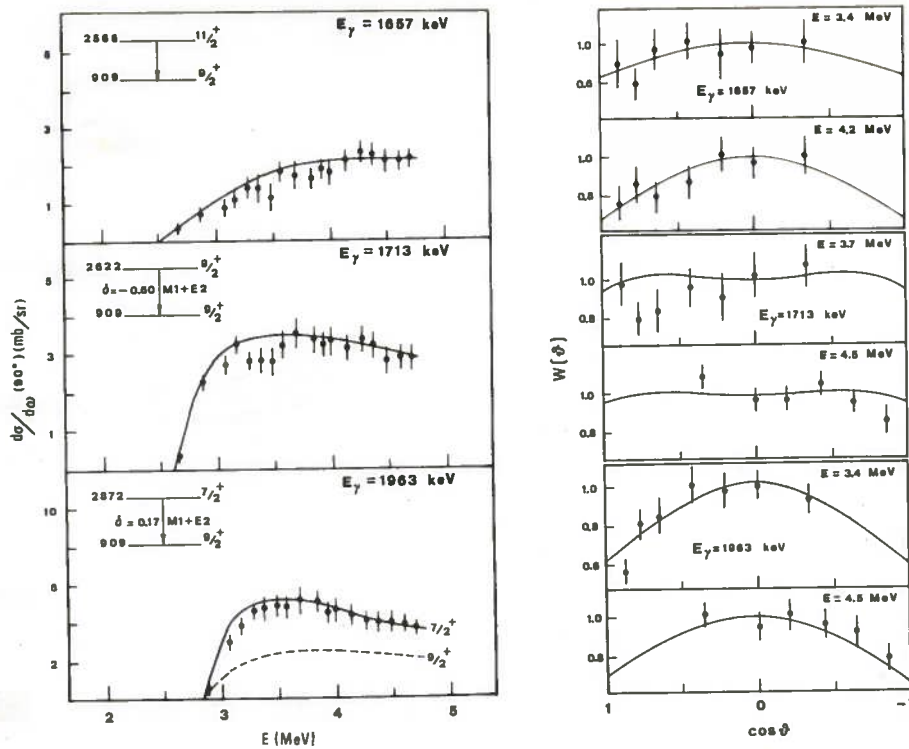


Fig.8-Experimental and calculated excitation functions (left panels) and angular distributions (right panels) of  $\gamma$ -decays from the 2566,2622 and 2872-keV levels. The solid curves are the calculations for the spin, parity, and  $\delta$ -values shown in the decay schemes. Other curves are theoretical calculations using various spins and parities.

The level at  $E_x=2881$  keV. The  $L=2$  transfer in the  $^{89}\text{Y}(p,p')$  reaction of ref. (5) implies  $J^\pi=(3/2,5/2)^-$  for this level, while a  $J^\pi=3/2^+$  assignment had tentatively been made in ref. (3). The angular distributions of the observed 2881-keV ground-state transition agree with  $J=3/2$ , whereas the excitation function favours a negative parity assignment (Fig. 9).

The level at  $E_x=2893$  keV. Clear evidence for a weak  $\gamma$ -ray of energy 1983.5 keV was observed in the present work only for neutron energies above 3.9 MeV. In our decay scheme this transition might be assigned only as a decay from the 2893-keV state observed in refs. (5)(12)(13) to the first excited state. The  $\gamma$ -ray yield measurements can well be extrapolated back to this threshold and agree with the assignment  $J^\pi=13/2^+$  proposed by Hultsman *et al.* (5). The positive anisotropy of the 1983.5 keV  $\gamma$ -ray supports this choice (Fig. 9).

The level at  $E_x=3067$  keV. A level at this energy was observed in refs. (5)(14). In refs. (3)(5) a  $J=3/2$  is suggested for this level, but the parity assignments are conflicting. In the present work we observed a ground-state transition together with a 1560-keV stop-over  $\gamma$ -ray. On the basis of the fits to the angular distributions of these two transi-

tions, the 3067-keV level has  $J=3/2$ . Both the experimental excitation functions are in better agreement with the calculations for a negative parity choice (Fig. 9).

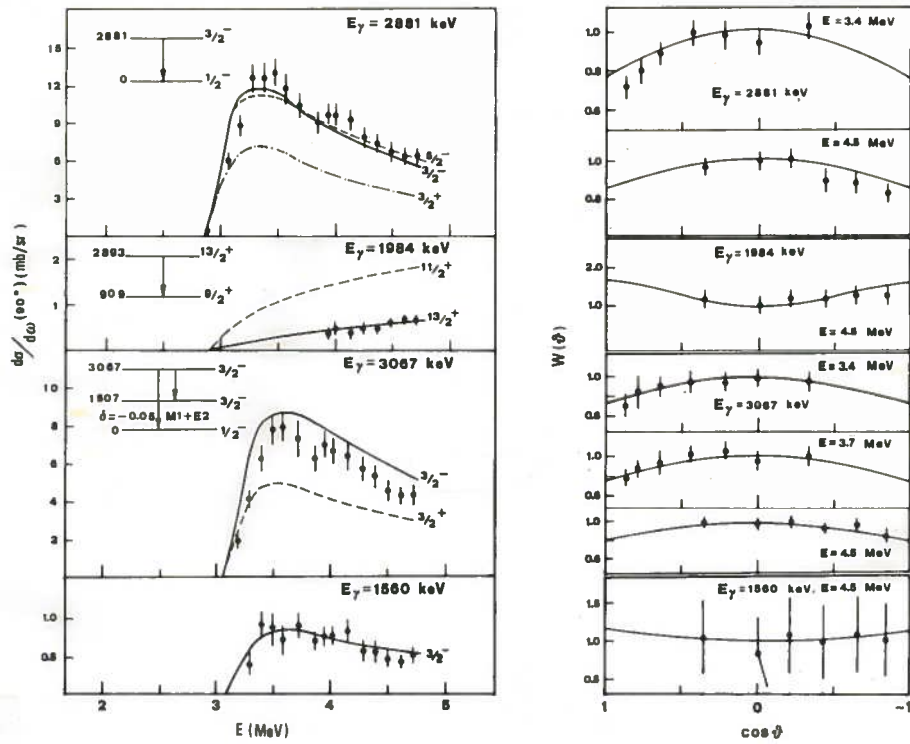


Fig.9-Experimental and calculated excitation functions (left panels) and angular distributions (right panels) of  $\gamma$ -decays from the 2881,2893,3067-keV levels. The notations for the curves are the same as in fig.8.

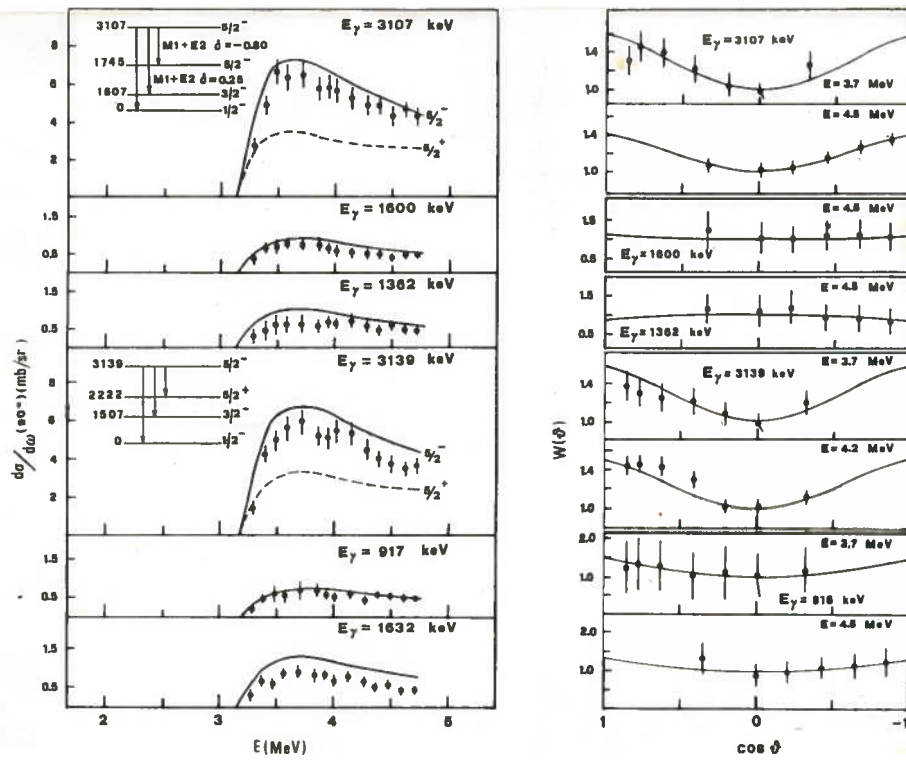


Fig.10-Experimental and calculated excitation functions (left panels) and angular distributions (right panels) of  $\gamma$ -decays from the 3107 and 3139-keV levels. The notations for the curves are the same as in fig.8.

The levels at  $E_x=3107$  and  $3139$  keV. Evidence for these two levels is reported in refs. (5)(11)(14). We attribute to both levels three possible decays, of which we studied the angular distributions and the excitation functions. The large positive anisotropy of the observed angular distributions to the ground state (Fig. 10) and HF cross section comparisons are consistent with the  $J^\pi=5/2^-$  spin assignment of ref. (5) for both levels. It should be noted that a positive parity assignment for these levels, as tentatively proposed in ref. (3) requires the ground-state transitions to be predominantly M2 and compete with dipole transitions, whereas the alternative assignment leads to the more likely E2-dipole competition.

The level at  $3247$  keV. A level at this energy was observed in ref. (5) but not assigned. In the present work, two decays have been attributed to it. The excitation functions of the  $3247$  and  $1740$ -keV decays are consistent with an assignment of both  $J^\pi=3/2^+$  and  $5/2^+$  (Fig. 11) whereas the angular distribution of the stop-over  $\gamma$ -ray favours the  $5/2^+$  choice.

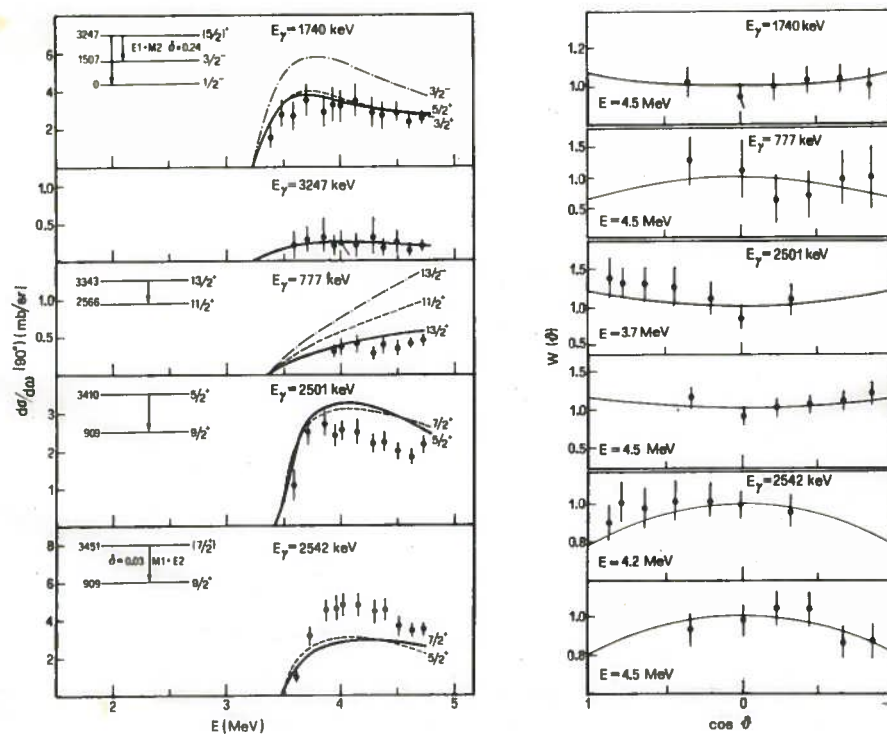


Fig.11-Experimental and calculated excitation functions (left panels) and angular distributions (right panels) of  $\gamma$ -decays from the  $3247, 3343, 3410$  and  $3451$ -keV levels. The notations for the curves are the same as in fig.8.

*The level at 3343 keV.* We have considered the 777-keV  $\gamma$ -ray observed for neutron energies above 3.9 Mev as the transition to the 2566-keV level from the high-spin state ( $J=13/2$ ) observed in refs. (12)(13). At lower bombarding energies the large background associated with the T(p,n) reaction precludes unambiguous threshold measurement. Multiple assignment for a  $\gamma$ -ray of this energy seems ruled out by selection rules. The calculation of the excitation function of the 777-keV  $\gamma$ -ray for  $J^\pi=13/2^+$  is in sufficient agreement with the experimental data (Fig. 11).

*The level at 3410 keV.* In ref. (3)  $J^\pi=5/2^+, 7/2$  are tentatively proposed for a level observed at this energy in refs. (5)(14). Both these spin values are in reasonable agreement with the excitation function of the 2501-keV  $\gamma$ -ray, whereas the positive anisotropy of the observed angular distributions is predicted only for  $J=3/2, 5/2$ . Hence  $J^\pi=5/2^+$  assignment is proposed for this level (Fig. 11).

*The level at 3451 keV.* In ref. (3)  $J^\pi=5/2^+, 7/2$  are tentatively proposed for a level observed at this energy in ref. (14). The comparison of measured and calculated excitation function for the observed 2542-keV  $\gamma$ -ray is inconsistent with both spin assignments. From the behaviour of the excitation function a cascade-feeding from higher levels can be excluded. The negative anisotropy of the observed angular distributions is predicted for  $J=7/2, 11/2$ . Because the choice 11/2 can be ruled out on the basis of cross section magnitude, the experiments favour the  $J^\pi=7/2^+$  assignment.

*The level at  $E_x=3503$  keV.* A level at this energy was observed in refs. (5)(14) but not assigned. Both the experimental excitation function and the angular distribution of the 1996-keV  $\gamma$ -ray are in agreement with the tentative suggestion  $J^\pi=7/2^+$  of ref. (3) for this level (Fig. 12).

*The level at  $E_x=3516$  keV.* This level must correspond to the 3511-keV level observed in ref. (14), and to the 3513-keV level observed in ref. (5). The L=2 transfer in (p,p') of ref. (5) implies  $J=3/2, 5/2$  and negative parity for this state. Both these values seem to be compatible with the excitation function of the observed ground-state transition but the parity is conflicting. The positive anisotropy of the 3516-keV  $\gamma$ -ray angular distribution is too weak when compared with the calculations for a quadrupole transition. Thus the choice 5/2 can be excluded. On this basis  $J^\pi=3/2^+$  can be assigned to this level (Fig. 12) as already proposed in ref. (3). A search for the mixing ratio for an E1-M2 mixture gives the result  $\delta=0.65^{+0.30}_{-0.15}$ .

*The level at  $E_x=3557$  keV.* A level at 3555 keV was weakly excited by the (p,p') reaction (5), but not assigned. In ref. (3)  $J^\pi=5/2^+$  is tentatively proposed for the level at 3559 keV observed in ref. (14), whereas in ref. (3) a tentative assignment of  $1/2^-$  is also

suggested. In the present work three  $\gamma$ -rays were found to originate from this level. The decay to the 909-keV state ( $J=9/2$ ) certainly eliminates  $1/2$  as a possible spin. While calculated excitation functions for  $J^\pi=5/2^+$  and  $7/2^+$  both agree with the measured values the least-squares fits to the angular distributions of the 2648 and 2050-keV  $\gamma$ -rays only agree with the distributions predicted for  $J=7/2$  (Fig. 12).

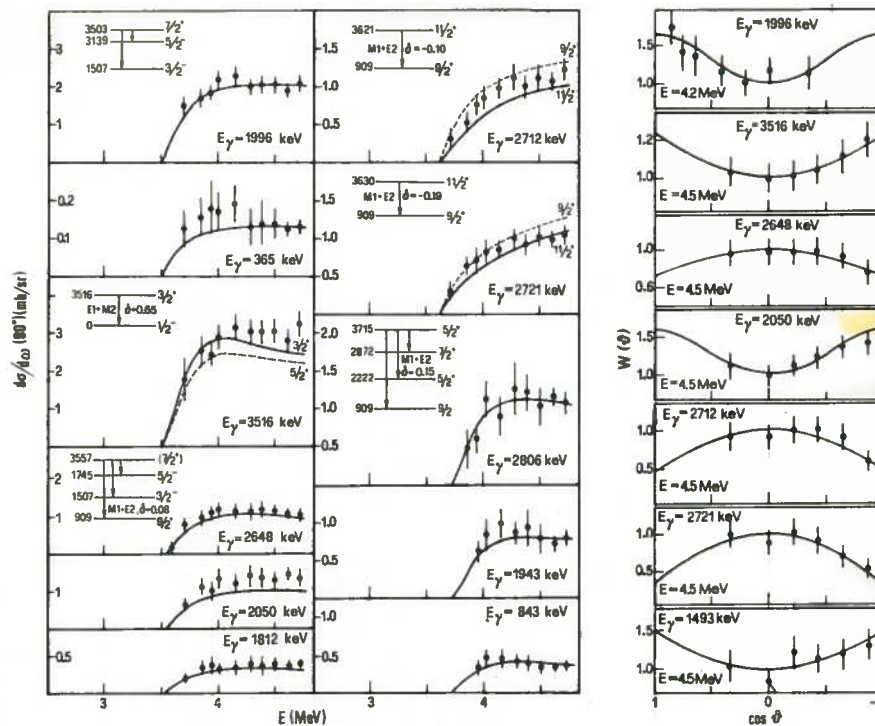


Fig.12-Experimental and calculated excitation functions (left panels) and angular distributions (right panels) of  $\gamma$ -decays from the 3503,3516,3557,3621,3630 and 3715 keV levels. The notations for the curves are the same as in fig.8.

The levels at  $E_x=3621$  and  $3630$  keV. The twofold multiplicity of the state near 3.63 MeV [refs. (5)(14)] was for the first time suggested in the present work (17). Because both the levels are excited with the same strength and present the same decay mode (Fig. 11), one expects to have the same spin. We have looked carefully for a decay of these levels to the ground state and found no such decay. Thus neither of them could be identified with the 3612-keV state from the (p, $\gamma$ ) work reported in ref. (3).

The experimental excitation functions agree with the calculations for  $J^\pi=(9/2,11/2)^+$ , whereas angular distribution comparison eliminates the  $9/2$  possibility. Hence  $J^\pi=11/2^+$  can be assigned to both the levels.

The level at  $E_x=3715$  keV. A level excited at this energy was observed in ref. (5) and assigned  $J^\pi=5/2^+$ . In ref. (3)  $J^\pi=9/2^+$  is tentatively proposed for the level at 3716 keV observed in ref. (14). In the present study this level is deexcited by three  $\gamma$ -rays. On

the basis of the cross section magnitude inferred for this level the possibility of  $J^\pi=9/2^+$  was ruled out. Both the angular distributions presented here for 1493-keV decay and the excitation functions support the  $5/2^+$  assignment.

*The levels at  $E_x=3748$  and  $3753$  keV.* According to Fig. 4, the  $\gamma$  peak shown at 2.84 MeV and with observed threshold at  $E=3.9$  MeV represents a group of two resolved lines. The 2838.7-keV  $\gamma$ -ray places a level at 3747.7 keV which might be identified with the state at 3750 keV [ $L=5$  in  $(p,p')$ ] of ref.(5).

The 3748-keV level was found to decay by only 2839-keV  $\gamma$ -ray. No evidence was found in the present work for a branching [ref. (3)] of this level. The present study indicates a  $J^\pi=9/2^+$  for this level. The 2844.2-keV  $\gamma$ -ray locates a new level at 3752.8 keV, which de-excites prominently by 2008-keV  $\gamma$ -ray. The threshold of the excitation function of the weak 342-keV  $\gamma$ -ray, as shown in Fig. 13, seems below  $E=3.75$  MeV. Thus the placement of this  $\gamma$ -ray in the scheme as the decay from the 3753-keV level to the 3410-keV level is tentative and is based only on its energy. On the other hand it does not possess enough strength to influence the possible spin assignment for the new level. Both the experimental excitation function and the angular distribution of the prominent 2008-keV  $\gamma$ -ray are well fitted by the calculation for  $J^\pi=5/2^+$  (Fig. 13).

*The level at 3848 keV.* The level must correspond to the 3852-keV observed in refs. (5)(14) and for which a tentative assignment of  $J^\pi=5/2^+$  is made in ref. (3). The excitation function and the angular distribution of the prominent 2103-keV decay have been studied: calculations with  $J^\pi=5/2^+$  give curves which are in sufficient agreement with the experimental data (Fig. 13).

*The level at 3862 keV.* A level at this energy was observed in refs. (5)(14). We attribute to it two possible decays, of which we studied the excitation function and the angular distribution. The large positive anisotropy of both the measured angular distributions (Fig. 13) excludes the  $J=3/2$  possibility of ref. (5) whereas the  $J^\pi=5/2^-$  is ruled out on the basis of cross section magnitude.

The best fit between measured and calculated quantities is obtained for  $J^\pi=7/2^+$  which does not conflict with  $\gamma$ -ray selection rules.

*The level at 3977 keV.* The observed 1447-keV weak  $\gamma$ -ray places a level at 3977 keV which might be identified with the state observed at 3957 keV in ref. (5) and assigned  $J=(9/2, 11/2)^+$ . The cross section of this decay favours the choice of  $J^\pi=11/2^+$  (Fig. 13).

*The level at 3991 keV.* In ref. (5)  $J^\pi=(3/2, 5/2)^-$  are suggested for this level. In this work we observed its ground-state transition. The choice of  $J^\pi=3/2^-$  is preferred on the basis of cross section magnitude (Fig. 13) whereas a non-unlikely mixing of M1 and E2

multipolarity of the observed 3991-keV  $\gamma$ -ray can account for the positive anisotropy of the angular distribution.

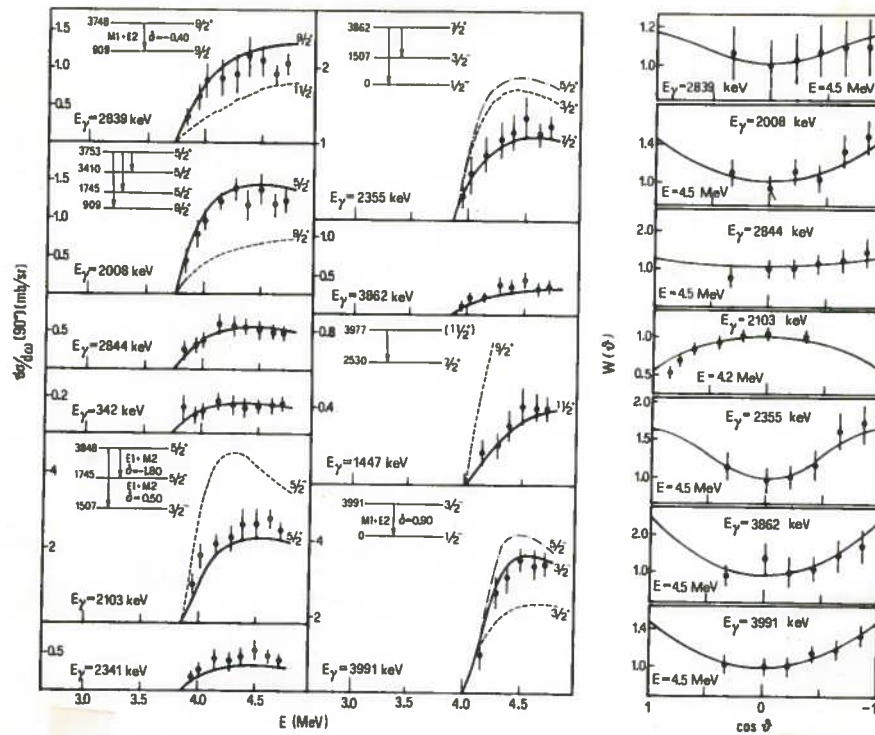


Fig.13-Experimental and calculated excitation functions (left panels) and angular distributions (right panels) of  $\gamma$ -decays from the 3748,3753,3848,3862,3977 and 3991 keV levels. The notations for the curves are the same as in fig.8.

*The level at 4015 keV.* The existence of a level at 4011 keV was established by a previous study (5) but no indication was given as to its spin. In this work the observed 4015.4-keV  $\gamma$ -ray can unambiguously be considered as the transition to the ground state from a level at this energy. By examining the branching ratio of its decay both  $J=1/2$  and  $J=3/2$  may be proposed according to  $\gamma$ -ray selection rules.

Neither of them are compatible with the low yields of the observed transitions (Fig. 14). In our work this is the only case of a complete failure of the cross section test for spin assignment. It should be noted, however, that our experiment does not allow for the exclusion of two other  $\gamma$ -decays which are energetically possible for the 4015-keV level but which are not distinguishable from two prominent lines present in all the spectra: the strong annihilation peak at 511 keV and the time-uncorrelated 909 keV  $\gamma$ -ray.

*The level at 4023 keV.* This level must correspond to the 4020-keV level observed in refs. (5)(14) and assigned  $J^\pi=(3/2,5/2)^-$ . In ref. (3)  $J^\pi=3/2^+$  is tentatively proposed. In the



present work, five decays have been attributed to this level. The HF calculated cross sections for  $J^\pi=5/2^-$  give values which are too high, whereas we obtain a more satisfactory agreement for  $J^\pi=3/2^-$ , which is consistent with the observed anisotropies of the angular distributions (Fig. 14).

*The level at 4105 keV.* The observed 3196-keV  $\gamma$ -ray confirms the existence of the state at 4104 keV reported in ref. (5), but not assigned.

In the present work this state has been attributed three decays. The experimental cross sections are in sufficient agreement with the calculated excitation curves for  $J^\pi=(5/2, 7/2)^+$ , whereas the angular distribution of the 3196-keV  $\gamma$ -ray seems to favour the choice of  $J^\pi=7/2^+$ , even if the associated errors are large (Fig. 14).

*The level at 4171 keV.* A level at this energy was observed in ref. (5), and assigned  $J^\pi=(3/2,5/2)^-$ . In the present work it was found to decay only to the ground state. The large positive anisotropy of the observed angular distribution excludes the  $J=3/2$  choice, whereas the study of the excitation function supports the  $J^\pi=5/2^-$  assignment (Fig. 14).

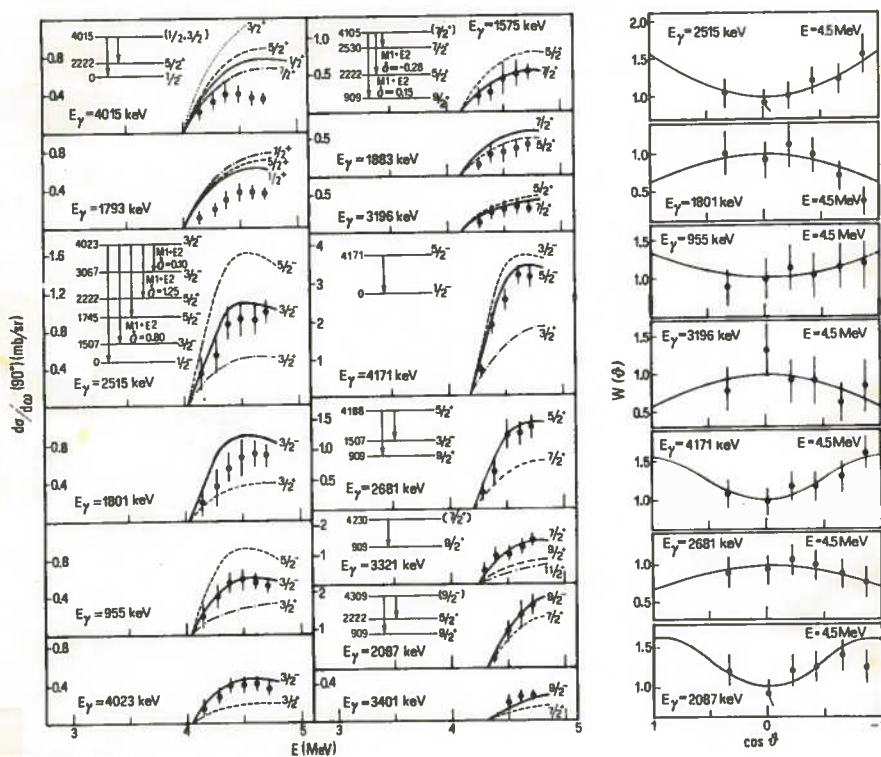


Fig.14-Experimental and calculated excitation functions (left panels) and angular distributions (right panels) of  $\gamma$ -decays from the 4015,4023,4105,4171,4230 and 4309 keV levels.The notations for the curves are the same as in fig.8.

*The level at 4188 keV.* A level at this energy was observed in ref. (5), and assigned  $J^\pi=5/2^+$ . In the present work the level decays through two observed  $\gamma$ -rays. Both the experimental excitation function and the angular distribution of the 2681-keV  $\gamma$ -ray confirm the  $J^\pi=5/2^+$  assignment (Fig. 14).

*The level at 4230 keV.* In ref. (5) a level at this energy was observed, but not assigned. In this experiment the good agreement of the excitation function threshold of the observed 3321-keV  $\gamma$ -ray confirms the existence of the reported level. Experimental cross sections for this level are shown in Fig. 14 together with calculated curves for  $J^\pi=(7/2, 9/2, 11/2)^+$ . A  $J^\pi=7/2^+$  assignment seems the most probable. The shape of the 3321-keV  $\gamma$ -peak, as shown in Fig. 2, suggests the presence of a weak unresolved component for which the peak-fitting procedure furnished the value of  $E_\gamma = 3326.2 \pm 1.9$  keV. So, on the basis of the excitation function threshold, the state reported at 4230 keV appears to be an unresolved doublet.

*The level at 4309 keV.* This level must correspond to the 4304-keV level observed in ref. (5), and assigned  $J^\pi=(7/2, 9/2)^-$ . In our work, it has been attributed two decays. Both the cross section and the angular distribution of the most intense decay ( $E_\gamma = 2087$  keV) favour the choice of  $J^\pi=9/2^-$  (Fig. 14).

Finally, in the energy region from 4.32 to 4.54 MeV, the present measurements confirm the existence of most of the states reported in ref. (5). Regarding the  $J^\pi$  assignments of these states we cannot make any confident statements, since the number of data points taken are not sufficient to pursue a meaningful excitation function study. Moreover, sensitivity limitations will probably cause weak transitions from these levels to be missed.

#### 4. - CONCLUSIONS

The  $^{89}\text{Y}$  excitation studies identified 69  $\gamma$ -rays, 29 of which were previously unreported, from 43 levels up to 4.54 MeV. Of these, the levels at  $E_x=3621$  and 3753 keV were observed for the first time in the present experiment. Some indication of multiplicity of the 4230-keV state is present. The proposed level scheme, shown in Fig. 5, generically confirms the one presented in Kockers's (3) compilation for  $^{89}\text{Y}$ . Spin and parity assignments for the levels below 4.32 MeV have been deduced on the basis of theoretical fits to the experimental excitation functions and angular distribution data. High-spin ( $J=13/2$ ) states below 4 MeV have been confirmed. New spin values are proposed for the levels at  $E_x=3247, 3410, 3451, 3503, 3557, 3621, 3753, 3848, 3862, 4015, 4105$  and 4230 keV.

REFERENCES

- (1) U. Abbondanno, F. Demanins, M.R. Malisan, and G. Nardelli, Nucl. Phys. A305 (1978) 117.
- (2) U. Abbondanno, A. Boiti, F. Demanins, C. Tuniz, and G. Nardelli, Nucl. Phys. A345 (1980) 174.
- (3) D.C. Kocher, Nucl. Data Sheets 16 (1975) 445
- (4) P.F. Hinrichsen, S.M. Shafroth, and D.M. Van Patter, Phys. Rev. 172 (1968) 1134
- (5) L. Hulstman, H.P. Blok, J. Verburg, J.G. Hoogteyling, C.B. Nederveen, H.T. Vijlbrief, E.J. Kaptein, S.W.L. Milo, and J. Blok, Nucl. Phys. A251 (1975) 269
- (6) E.W. Hamburger, Nucl. Phys. 39 (1962) 139
- (7) J. Alster, D.C. Shreve, and R.J. Peterson, Phys. Rev. 144 (1966) 999
- (8) J.H. Towle, Nucl. Phys. A131 (1969) 561
- (9) S.M. Shafroth, P.N. Trehan, and D.M. Van Patter, Phys. Rev. 129 (1963) 704
- (10) Patricia S. Buchanan, Suresh C. Mathur, W.E. Tucker, and I.L. Morgan, Phys. Rev. 158 (1967) 1041
- (11) C. Budtz-Jørgensen, P. Guenther, A. Smith, and J. Whalen, Z. Phys. A-Atoms and Nuclei 319 (1984) 47
- (12) M. Davidson and J. Davidson, M. Behar, G. Carcia Bermudez, and M.A.J. Mariscotti, Nucl. Phys. A306 (1978) 113
- (13) C.A. Fields, and L.E. Samuelson, Phys. Rev. C20 (1979) 2442
- (14) Patricia S. Buchanan and G.H. Williams, Bull. Am. Phys. Soc. 13 (1968) 873
- (15) W. Hauser and H. Feshbach, Phys. Rev. 87 (1952) 366
- (16) G.R. Satchler, Phys. Rev. 94 (1954) 1304; 104 (1956) 1198; 111 (1958) 1747 (E)
- (17) G. Nardelli, P. Pavan, and G. Torielli, Nuovo Cim. Lett. 38 (1983) 129
- (18) L.E. Beghian, F. Hoffmann, and S. Wilensky, Nucl. Instr. 41 (1966) 141
- (19) P. Menon, Thesis, Istituto di Fisica (Padova, 1978)
- (20) C.M. Lederer and V.S. Shirley, Tables of Isotopes, 7th ed. (Wiley, New York, 1978)
- (21) R.E. Azuma, L.E. Carlson, A.M. Charlesworth, K.P. Jackson, N. Anyas Weiss and B. Lalovic, Can. J. Phys. 44 (1966) 3075
- (22) E. Storm, and H.I. Israel, Nucl. Data Tables A7 (1970) 565
- (23) C.A. Engelbrecht, Nucl. Instr. 93 (1971) 103
- (24) Neutron Data from CCDN files, NEA Data Bank, B.P.9, F-91190 Gif-sur-Yvette, France
- (25) M.T. McEllistrem, in Nuclear Research with Low Energy Accelerators, edited by J.B. Marion and D.M. Van Patter (Academic, New York, 1967), pp. 167 and 168
- (26) F.D. McDaniels, G.P. Glasgow, and M.T. McEllistrem, Proceedings of the International Conference on Nuclear Cross Sections for Technology (Knoxville, TN, USA, 1979) edited by J.L. Fowler and C.N. Johnson (Washington, DC, USA:NBS 1980) p. 182
- (27) F. Demanins, and G. Nardelli, INFN Report BE-70/3
- (28) H. Liskien, and A. Paulsen, Nucl. Data Tables 11 (1973) 569
- (29) U. Fasoli, A. Metellini, D. Toniolo, and G. Zago, Nucl. Phys. A205 (1973) 305
- (30) F.D. Becchetti, Jr. and G.W. Greenless, Phys. Rev. 182 (1969) 1190
- (31) D. Wilmore and P.E. Hodgson, Nucl. Phys. 55 (1964) 673
- (32) C.M. Perey, and F.G. Perey, Nucl. Data Tables 17 (1976) p. 5
- (33) E.H. Auerbach, Brookhaven National Laboratory report BNL 65/62 (1964)
- (34) E. Sheldon, S. Mathur, and D. Donati, Comp. Phys. Comm. 2 (1971)272
- (35) P.A. Moldauer, Phys. Rev. 123 (1961) 968
- (36) A.M. Lane, J.E. Lynn, E. Melkonian, and E.R. Rae, Phys. Rev. Lett. 2 (1959) 424
- (37) C.H. Johnson, A. Galonsky, and R.L. Kernell, Phys. Rev. Lett. 39 (1977) 1604
- (38) M.D. Goldberg, S.F. Mughabghab, B.A. Magurno, and V.M. May, Brookhaven National Laboratory report BNL 325, Vol. IIA, 1966
- (39) E. Sheldon, and D.M. Van Patter, Rev. Mod. Phys. 38 (1966) 143